AGU PUBLICATIONS

JGR

Journal of Geophysical Research: Space Physics

RESEARCH ARTICLE
10.1002/2016JA023136

Key Points:
- The AGILE satellite observed more TGFs originating from the same spatially limited geographic regions
- This work represents an indirect evidence that more TGFs can be produced by thunderstorms throughout their lifetime
- The orbit of the AGILE satellite is unique to perform follow-up of thunderstorms in time

Correspondence to:
A. Ursi,
alessandro.ursi@iaps.inaf.it

Citation:
Ursi, A., M. Marisaldi, M. Tavani, D. Casella, P. Sanò, and S. Dietrich (2016), Detection of multiple terrestrial gamma-ray flashes from thunderstorm systems, *J. Geophys. Res. Space Physics*, *121*, 11,302–11,315, doi:10.1002/2016JA023136.

Received 6 JUL 2016
Accepted 5 OCT 2016
Accepted article online 7 OCT 2016
Published online 9 NOV 2016

Detection of multiple terrestrial gamma-ray flashes from thunderstorm systems

A. Ursi[1,2], M. Marisaldi[3,4], M. Tavani[1,2], D. Casella[5], P. Sanò[5], and S. Dietrich[5]

[1]INAF-IAPS, National Institute for Astrophysics, Rome, Italy, [2]Department of Physics, University of Roma Tor Vergata, Rome, Italy, [3]INAF-IASF, National Institute for Astrophysics, Bologna, Italy, [4]Birkeland Centre for Space Science, University of Bergen, Bergen, Norway, [5]ISAC-CNR, Institute for Atmospheric Science and Climate, Rome, Italy

Abstract Since their discovery, Terrestrial Gamma ray Flashes (TGFs) exhibited an evident correlation with thunderstorms and lightning activity. The fleeting nature of these events and the heavy absorption of gamma rays in the lowest atmospheric layers severely hamper the observation of this phenomenon, making us reveal just a small fraction of a probably much wider population. As each thunderstorm produces a large amount of lightning discharges during its lifetime, it is reasonable that even a large amount of TGFs are produced during the same event. However, detection of multiple TGFs coming from the same storm is difficult to perform, as it requires the constant monitoring of a spatially limited geographic region: this is not an easy task to perform for satellites on high-inclination orbits that make them experience nonnegligible latitudinal shifts at each orbital passage over a certain region, preventing the monitoring of a limited geographic region throughout successive overpasses. In this perspective, the quasi-equatorial (2.5°) orbit of the Astrorivelatore Gamma ad Immagini LEggero (AGILE) satellite ensures a minimal latitudinal shift when flying over the same region at successive passages, allowing for the follow-up of thunderstorms in time. We exploit this feature of the AGILE satellite to search for multiple TGFs coming from the same geographic region and, in particular, from the same thunderstorm. We carry out this search on the AGILE TGF database (2009–2016), ending up with a sample of 79 systems producing more than one TGF, both during the same overpass and up to four overpasses after. Data acquired by geostationary meteorological satellites and cross correlation with radio sferics detected by World Wide Lightning Location Network are used to support this investigation. The AGILE satellite for the first time clearly establishes the multiple occurrences of TGFs from convective thunderstorms, both on timescales of minutes to several hours.

1. Introduction

Terrestrial Gamma ray Flashes (TGFs) are submillisecond intense gamma ray flashes occurring in the Earth atmosphere, strictly correlated with convective thunderstorms and electric activity. Unexpectedly discovered in the early 1990s by the Compton Gamma Ray Observatory (CGRO) [*Fishman et al.*, 1994], these elusive events have been further investigated by several satellites devoted to high-energy astrophysics, such as the Reuven Ramaty High-Energy Spectroscopic Imager (RHESSI) [*Smith et al.*, 2005; *Grefenstette et al.*, 2009], the Astrorivelatore Gamma ad Immagini LEggero (AGILE) [*Marisaldi*, 2010a, 2010b], and the Fermi Space Telescope [*Briggs et al.*, 2010].

TGFs exhibit an average time duration of ∼100 μs [*Briggs et al.*, 2013] and energies ranging from few keV to several tens of MeV. In particular, the AGILE satellite reported observations of energies up to 100 MeV [*Tavani et al.*, 2011]. The geographic distribution of TGFs strongly reflects the global lightning distribution, clustering over land and within the tropical belt, where thunderstorms are more frequent and intense and where the tropopause is higher, making it easier for the gamma rays to escape to space.

Simulations of gamma ray propagation and absorption in the atmosphere place the TGF source altitude between 10 km and 15 km above sea level [*Dwyer and Smith*, 2005; *Stanley et al.*, 2006; *Shao et al.*, 2010; *Lu et al.*, 2010]. The association with thunderstorms has been further confirmed by studying one-by-one correlations between TGFs and individual lightning strokes: this can be performed by taking advantage of temporal and spatial coincidences with very low frequency radio waves emitted by lightning [*Connaughton et al.*, 2010, 2013].

TGFs are believed to be bremsstrahlung gamma ray emissions, produced by avalanches of electrons accelerated to relativistic energies within thunderstorm strong electric fields [*Gurevich et al.*, 1992; *Dwyer*, 2008, 2012]. Such electric field may be found at the tip of stepped leaders, during the lightning process: in this view, each lightning stroke may, in principle, produce an associated TGF. Several studies investigated the meteorological scenario associated to the TGF production, showing that TGFs follow the diurnal, seasonal, and geographic patterns of lightning activity on Earth and are associated with tall (13–17 km) tropical thunderstorms [*Splitt et al.*, 2010], with rare conditions of flash rate, Convective Available Potential Energy (CAPE) amount and cloud extension [*Fabró et al.*, 2015]. On the basis of radar observations, it seems there are no privileged thunderstorm conditions for TGF production [*Chronis et al.*, 2016]. On the other hand, tropopause height seems to play an important, but not dominant role, in the TGF geographic distribution [*Smith et al.*, 2010] and the TGF sample cannot be fully considered a subset of the lightning stroke sample, as there exist some regional discrepancies in the two distributions [*Fuschino et al.*, 2011]. Investigations on the intrinsic brightness of TGFs also reveal that the source region should be placed in the interior of the thunderstorm, between the two main charge layers [*Cummer et al.*, 2014].

While several studies have been performed to characterize the physical properties of thunderstorms producing TGFs, no investigations have been carried out to establish whether single thunderstorms actually produce multiple TGFs. Motivated by this possibility, we carried out a search for multiple TGFs in the AGILE TGF data set, covering the period from 1 March 2009 to 13 March 2016, and we deeply analyzed these events, to see whether there is evidence of more TGFs coming from the same thunderstorm. Moreover, we tried to establish whether these events tend to occur during a specific phase of the thunderstorm evolution.

We used the AGILE TGF data set to identify TGFs coming from approximately the same geographical region (see section 3), and the meteodata products described above to characterize the thunderstorm activity and its time evolution around the TGF location. The peculiar AGILE capability to observe the same region in successive orbital passages is described in detail in section 2.1.

2. The AGILE Satellite

The Astrorivelatore Gamma ad Immagini LEggero (AGILE) [*Tavani and othes*, 2009] is a small mission of the Italian Space Agency (ASI), devoted to high-energy astrophysics. AGILE was launched on 23 April 2007 from Satish Dhawan Space Centre (India) on a PSLV rocket and put in a low inclination (2.5°) equatorial Low-Earth Orbit at 540 km altitude.

The AGILE payload is composed of three instruments: a tungsten-Silicon Tracker (ST) gamma ray imager, a silicon-based X-ray detector SuperAgile (SA), and a MiniCalorimeter (MCAL) [*Labanti et al.*, 2009]. All instruments are surrounded by an AntiCoincidence (AC) system.

All detectors aimed at studying TGFs are affected by dead time, due to the very short duration and high fluence ($\sim$0.1 ph cm^{-2}) of these events. The AGILE AC modulus induced a nonnegligible dead time effect on the detection of TGFs as well [*Marisaldi et al.*, 2014], leading to a loss of short-duration TGFs (<100 μs) and preventing any kind of correlation between TGFs and sferic radio waves emitted by lightning strokes. Since 23 March 2015, the AGILE onboard software configuration was modified and the AC veto signal on the MCAL detector was permanently disabled [*Marisaldi et al.*, 2015], leaving all the other trigger parameters and off-line selection criteria unvaried. Such changes lead to an increase in the sensitivity to TGFs of about one order of magnitude with respect to the previous configuration, from $\sim$10 TGFs/month up to $\sim$100 TGFs/month.

In 6 years activity, from 1 March 2009 to 22 March 2015, the AGILE satellite detected a total of 498 TGFs. With the enhanced configuration, from 23 March 2015 to 13 March 2016, with a lack of data for the month of September due to technical issues, the AGILE satellite detected a total of 648 TGFs. This represents the highest detection rate (TGF/km^2/yr) to date for any satellite. Physical features (longitude distribution, local time variation, and number of counts) of the new TGF population are consistent with the previously detected sample, except for a larger fraction of events exhibiting a shorter duration (<100 μs). As a consequence, throughout the enhanced configuration TGF data sample, 39 matches with the World Wide Lightning Location Network (WWLLN) radio sferics were found, with a delay between TGF and sferic $\Delta t \leq 200\mu$s, as the probability of finding a correlated sferic is inversely proportional to the TGF duration.

At the moment, AGILE is the only satellite whose TGF data set is permanently linked with meterological information. A nearly real time pipeline to retrieve and process meteorological images acquired by weather

satellites has been recently established, aimed at investigating the geographic region where the TGF events took place. This system exploits data by geostationary satellites, such as the Meteosat Second Generation (MSG) series, the Geostationary Operational Environmental Satellite (GOES) series, and the Himawari series of the Japan Meteorological Agency (JMA), as well as by Low-Earth Orbit (LEO) satellites, whenever possible, providing a constant monitoring of thunderstorm active regions, such as central Africa, the Maritime Continent, and northern South America.

One of the products of this pipeline is the identification of convection by means of the Global Convective Diagnostics (GCD) algorithm [*Mosher*, 2001; *Martin et al.*, 2008], a simple technique based on the brightness temperature difference between the ~11 μm infrared (IR) and the ~6 μm water vapor (WV) channels, both available on all geostationary weather satellites. In condition of no convection, this parameter is GCD ≥ 0 K, while in case of convection it becomes GCD ~ 0 K; moreover, in case of deep convection, for particularly intense updrafts, this parameter is even GCD ≤ 0 K. Other products are the Cloud Top Temperature (CTT), which can be inferred from the T_{IR} brightness temperature, and the Cloud Top Height (CTH), available for the MSG data.

2.1. Advantages of the AGILE Orbit

The AGILE quasi-equatorial orbit has the smallest inclination (2.5°) ever achieved by a high-energy astrophysics mission. This not only has an important role in ensuring a low charged particle background, but it also puts the satellite in a privileged position for what concerns the *detection of more TGFs coming from the same thunderstorm*.

With respect to other satellites currently detecting TGFs, such as RHESSI (orbital inclination of 38°) and the Fermi Space Telescope (orbital inclination of 25.6°, the AGILE orbit experiences a very small (≤ 1°) latitude shift when overpassing the same longitude region after a whole orbit: this allows for the monitoring of a restricted geographical region on the equator, even throughout an extended time interval. As tropical convective systems typically exhibit spatial extensions of few squared degrees and last several hours, the possibility of flying over the same region at successive orbits represents a powerful tool to detect more TGFs coming from the same still active source.

The projection of a satellite orbit on Earth's surface can be approximated by a sinusoidal wave in geographic coordinates:

$$\varphi(\lambda) = \varphi_i \cdot \sin(\lambda) + \varphi_0 \tag{1}$$

where λ is the geographic longitude, φ is the geographic latitude, φ_i is the orbital inclination, and φ_0 is an arbitrary phase. The period T corresponds to the time required for the spacecraft to complete a whole orbit around the globe. Due to the Earth rotation, at the end of one full orbit the satellite footprint on the Earth surface will be in a different position. Taking as starting point the coordinate center ($\lambda = 0°$, $\varphi = 0)°$, given a satellite velocity ω_{SAT} and an Earth angular velocity $\omega_E \sim 0.25°$/min, after one period T, a satellite will find itself longitudinally shifted from its starting position by a quantity $-\Delta\lambda = \omega_E \cdot T$. It will take a certain time interval $\Delta t = \Delta\lambda \cdot [\omega_{SAT} \cos(\varphi_i)]^{-1}$ to fill this longitude gap and complete an effective whole revolution around the Earth. At this point, the satellite will occupy the same longitude, but a different latitude, depending on the orbital inclination φ_i. This latitude shift will be equal to

$$\Delta\varphi = \varphi_i \cdot \sin(\Delta\lambda) \tag{2}$$

Taking into consideration the three spacecraft currently detecting TGFs, we notice that after a complete revolution RHESSI and Fermi would experience a latitudinal shift of $\Delta\varphi_{RHESSI} \sim 15°$ and $\Delta\varphi_{Fermi} \sim 10°$, respectively, while the AGILE satellite would undergo a much smaller variation of just $\Delta\varphi_{AGILE} \sim 1°$. The parameter $\Delta\varphi$ is crucial for what concerns the monitoring of a certain restricted area, as it represents the northward/southward shift a spacecraft would experience when returning over the same geographic region at successive passages and it is fundamental for performing successive observations of spatially limited thunderstorm systems. In Figure 1 the projections of the orbits of RHESSI, Fermi, and AGILE on Earth's surface are shown. It is evident that the AGILE orbit is the only one that crosses the region of interest even in the successive orbit, given the smaller inclination.

The time required for the AGILE satellite to return over the same longitude after one orbit and compensate the spatial shift $\Delta\lambda$ will be equal to the orbital period $T \sim 94.3$ min plus the time delay $\Delta t \sim 6.2$ min, that is the effective period of the satellite $T_{eff} \sim 100.5$ min.

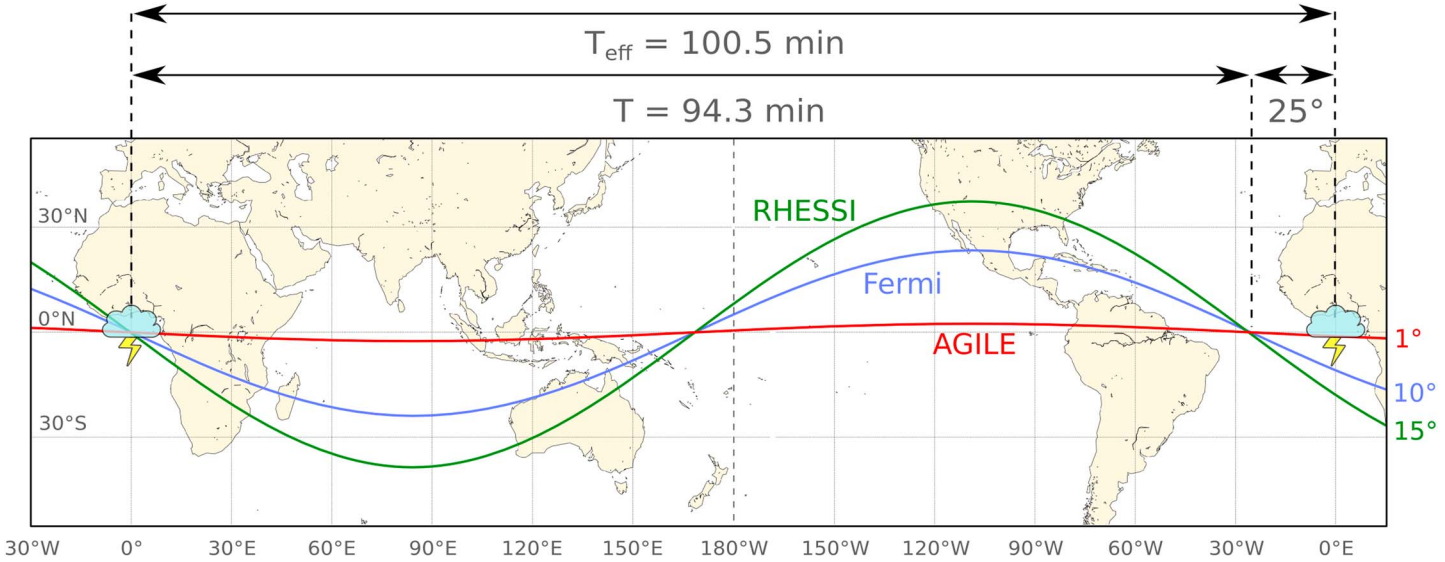

Figure 1. Projections of RHESSI, Fermi, and AGILE orbits on Earth's surface. The period of the sinusoidal waves does not coincide with a whole orbital revolution, resulting in a longitude shift $\Delta\lambda$. The AGILE orbit is the only one allowing the observation of the same thunderstorm region, even on successive passages, every 100 min. In the figure, we show an example of a site in the Gulf of Guinea that is assumed to be observed by AGILE, Fermi, and RHESSI in a first pass, but that subsequently can be repeatedly observed only by AGILE.

3. Multiple TGFs

The search for multiple TGFs in the AGILE data set is carried out by selecting all events coming from the same spatially limited geographic region, both during the same orbital passage and at successive overpasses on that region. To do that, the waiting time distribution of all detected TGFs is taken into consideration, and all events whose time separation is less than 1 min or equal to the time at which successive orbital resonances take place are selected as multiple TGF candidates. In order to characterize the meteorological scenario associated to these events and possibly identify the thunderstorm source, data acquired by geostationary satellites are also used and processed, with particular attention to algorithms aimed at identifying convection in the atmosphere. Finally, a cross search for sferic counterparts is carried out, by using the WWLLN database.

We treat the standard and the enhanced AGILE detection configurations separately, as they are characterized by different detection rates. In Figure 2, the distribution of waiting times τ between each pair of consecutively detected TGFs is plotted, for the standard (a) and the enhanced (b) detection configuration, with a binwidth of 1 min. Both configurations show enhancements at $\tau \leq 1$ min and $\tau \sim nT_{\mathrm{eff}}$ (with $n = 1, 2, 3$), corresponding to TGFs detected during the same passage of the AGILE satellite and at the successive effective periods, respectively. The enhanced configuration shows wider peaks, due to the increased statistics given by the highest detection rate, resulting in a more populated distribution for each waiting time value. As the AGILE satellite travels at an average velocity of 3.6°/min, the 1 min wide binning ensures that the two footprints lie within 3.6°, that is within about 400 km. We skim only the TGFs whose footprints lie within 300 km, in order to consider events coming from a spatially limited region, more likely produced by a unique thunderstorm system.

Among the 498 TGFs of the standard configuration sample, we identify five pairs of consecutive events with $\tau \leq 1$ min, five pairs of events with $\tau \sim T_{\mathrm{eff}}$, and three pairs of events with $\tau \sim 2 \cdot T_{\mathrm{eff}}$; on the other hand, among the 648 TGFs of the new sample, we identify 21 pairs of consecutive events with $\tau \leq 1$ min, 22 pairs of events with $\tau \sim T_{\mathrm{eff}}$, and 17 pairs of events with $\tau \sim 2 \cdot T_{\mathrm{eff}}$. Cases are present of either $\geq$2 TGFs detected during the same passage or of more TGFs detected after several overpasses. From a statistical point of view, we take a homogeneous Poisson distribution $e^{-\mu t}$, with μ frequency at which events take place, in order to characterize the expected behavior of a TGFs randomly distributed in time. In the standard configuration, the AGILE MCAL detected 498 TGFs in more than 6 years activity, which corresponds to a detection rate of about 1 order of magnitude smaller $\mu \sim 1.6 \cdot 10^{-4}$ TGFs/min. The probability that the three enhancements at $\tau \leq 1$ min,

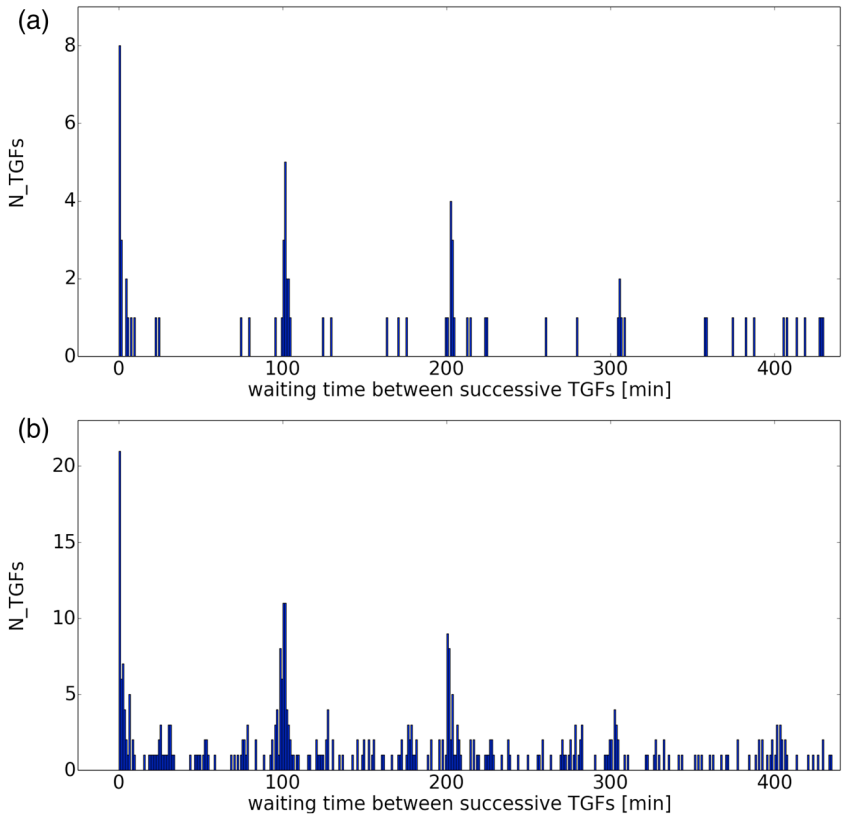

Figure 2. Distribution of waiting times between each pair of consecutively detected TGFs, for (a) the standard and (b) the enhanced detection configuration. Enhancements are evident for TGF pairs occurring within 1 min one from the other and at the first three orbital resonances ($\tau \leq 1$ min, $\tau \sim 101$ min, and $\tau \sim 202$ min), corresponding to TGFs detected during the same passage, after one overpass and after two overpasses, respectively. An increase in the number of detected TGFs is clear in the distribution for the enhanced configuration, which shows higher statistics.

$\tau \sim T_{\text{eff}}$, and $\tau \sim 2 \cdot T_{\text{eff}}$ were produced by statistical fluctuations are equal to $p \sim 1.6 \cdot 10^{-8}$, $p \sim 2.1 \cdot 10^{-10}$, and $p \sim 2.2 \cdot 10^{-5}$, respectively. In the enhanced configuration, the AGILE MCAL detected 648 TGFs in almost 10 months activity, with a lack of data for the month of September due to technical problems, that corresponds to $\mu \sim 1.38 \cdot 10^{-3}$ TGFs/min. The highest statistics of this sample strongly affects the probability of statistical fluctuations in the background rate: the number of expected TGF pairs taking place within 1 min is 0.9 and the corresponding probability to have a statistical fluctuation equal to 21 TGF pairs from a Poisson distribution is $p \sim 8.1 \cdot 10^{-22}$. Similarly, the probability of having 22 pairs of events within $\tau \sim T_{\text{eff}}$ and 17 pairs of events within $\tau \sim 2 \cdot T_{\text{eff}}$ given by statistical fluctuations is equal to $p \sim 3.3 \cdot 10^{-18}$ and $p \sim 1.3 \cdot 10^{-13}$, respectively. These enhancements are then clearly not statistical fluctuations but are produced by the presence of long lasting and extended thunderstorms in certain geographical regions, such as central Africa and the Maritime Continent. This does not imply that these TGF pairs are produced by the same thundercloud, as 1 min wide bins in our waiting time distribution translates into a maximum distance between the detected events of about 1800 km, taking into account an orbital satellite velocity of 3.6°/min and uncertainty circles with radius ~700 km around each detected TGF. In order to better investigate these regions, we limit the distance between the events belonging to each TGF pair by skimming only those whose satellite footprints lie at less than 300 km. In the standard configuration, 35 TGFs have been detected, belonging to 18 different passages over a stormy region: 5 out of them produced more TGFs that have been detected by AGILE during the same orbital passage, while the remaining 13 produced repeated TGFs, detected up to three overpasses after. The enhanced configuration is characterized by higher statistics and allowed for the detection of 127 TGFs, belonging to 61 different convective extended systems: 23 out of them produced more TGFs detected during the same passage, 38 out of them produced more TGFs detected up to four overpasses after. Also, three mixed cases of TGFs detected either during the same passage and the successive overpasses have been found.

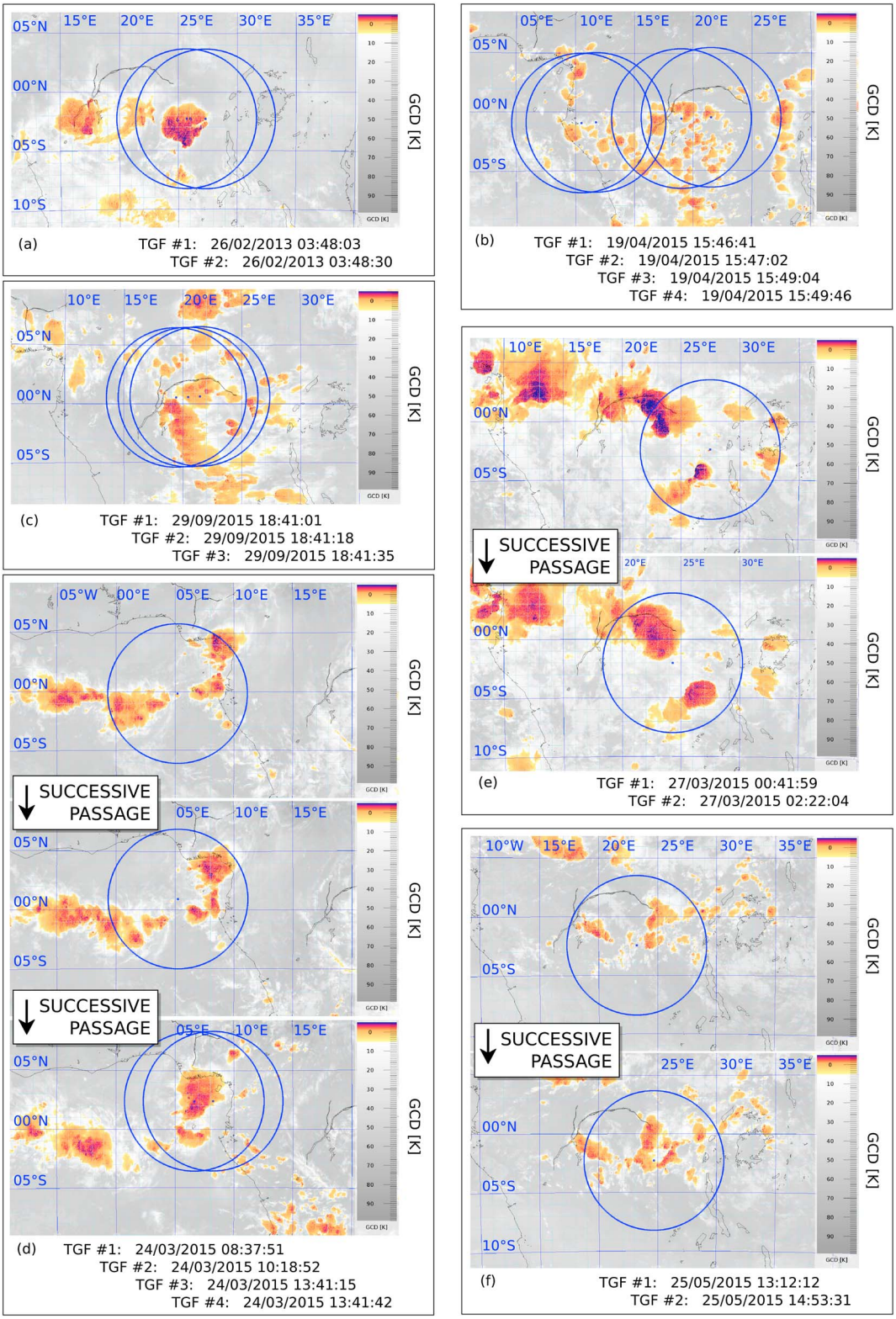

Figure 3. Examples of consecutive TGFs detected by AGILE and related (within 15 min from the TGF time) maps of GCD values acquired by geostationary satellites. Circles are centered at the spacecraft footprint at the detection time and have a ~700 km radius. (a–c) Consecutive TGFs detected during the same orbital passage over a convective region; (d–f) TGFs coming from the same thunderstorm system, detected at the successive orbital overpass.

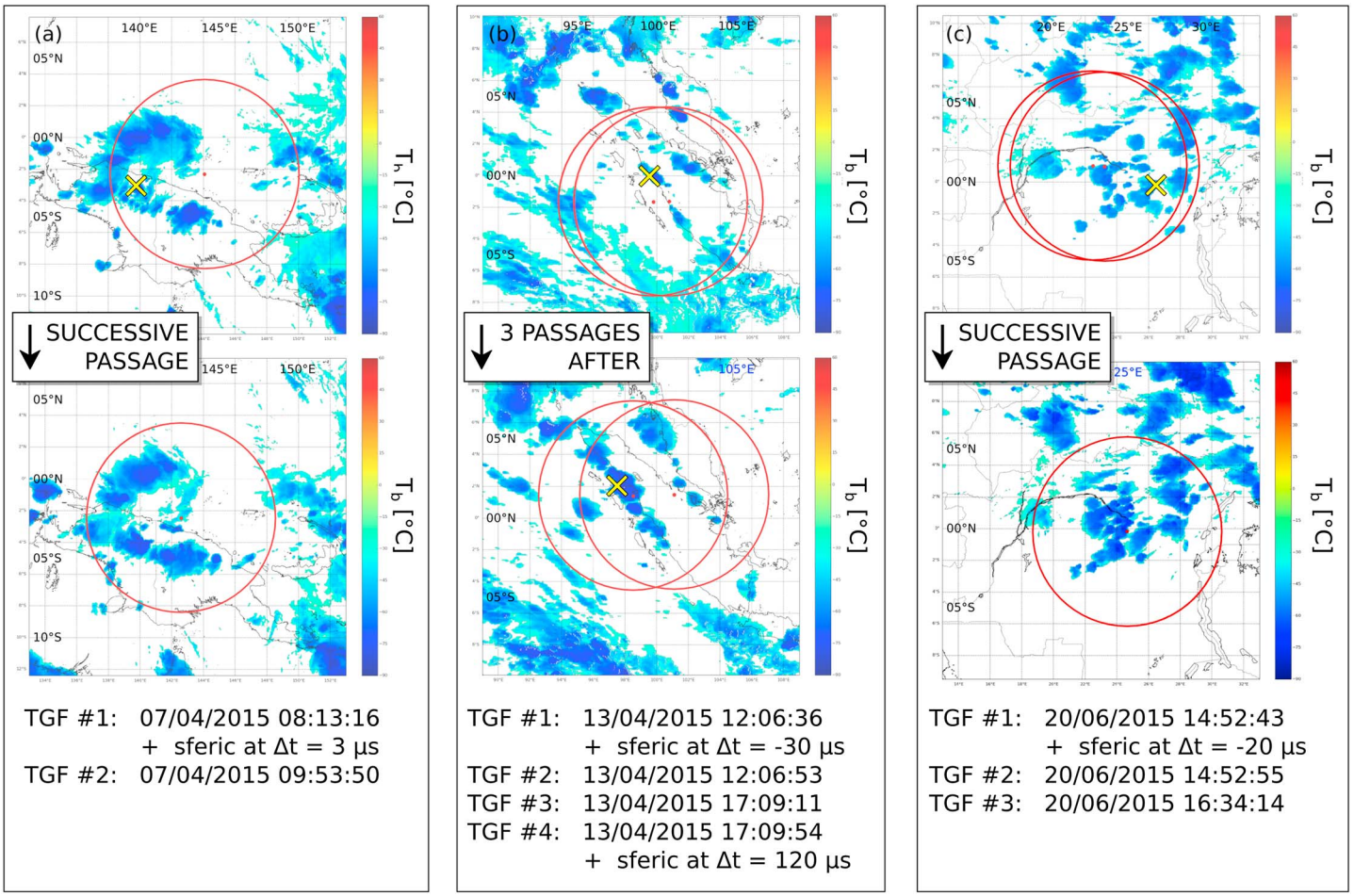

Figure 4. Three cases of multiple TGFs with correlated radio sferics by the WWLLN. (a, c) TGF pairs separated in time by one orbital period, with one sferic taking place during the first or the second passage. (b) Two pairs of successively detected TGFs (red dots), separated in time by three orbital periods, on 13 April 2015, with two correlated sferics. A first WWLLN sferic (yellow cross), occurring 30 μs before the first TGF of the first pair, and another sferic was found, occurring 120 μs after the second TGF of the second pair. The meteorological images acquired by the MT-SAT2 satellite show the IR 10.8μm brightness temperature, corresponding to the cloud top temperature: lower temperatures correspond to higher regions in the image and to the formation of a convective system. These images highlight a thunderstorm system evolving in time along the western coast of Sumatra.

4. Sferic Counterparts

We take advantage of images acquired by meteorological satellites to take a look to the meteorological scenario in which those events took place. Figure 3 shows examples of meteorological images, related to the discussed TGF sample, highlighting underlying extended convective systems by means of the GCD algorithm: central red dots correspond to the satellite footprint at the detection time, surrounded by ~700 km radius uncertainty circles. Figures 3a–3c represent multiple TGFs (up to four consecutive events) detected during the same orbital passage, while Figures 3d–3f represent multiple TGFs detected throughout successive overpasses (up to three effective periods after). In particular, case (d) is a mixture of TGFs detected either at successive passages or during the same passage. Convection is always present in the region where the AGILE multiple TGFs were revealed and this confirms that tropical thunderstorm systems are active for several hours, possibly emitting lightning and TGFs.

In order to identify the source cloud, we performed a search for sferics, for the discussed TGF sample, throughout the WWLLN database; such search was carried out for the period between 23 March 2015 and 23 June 2015. For the previous period with standard configuration, WWLLN sferic counterparts were not found [*Marisaldi et al.*, 2014], while for the successive period due to a degradation of the timing accuracy still under study: as a consequence, out of the 138 total AGILE TGFs selected for the current paper, only 6 sferics have been identified. Unfortunately, these sferics match single TGFs of different multiple TGF subsets: that is, no

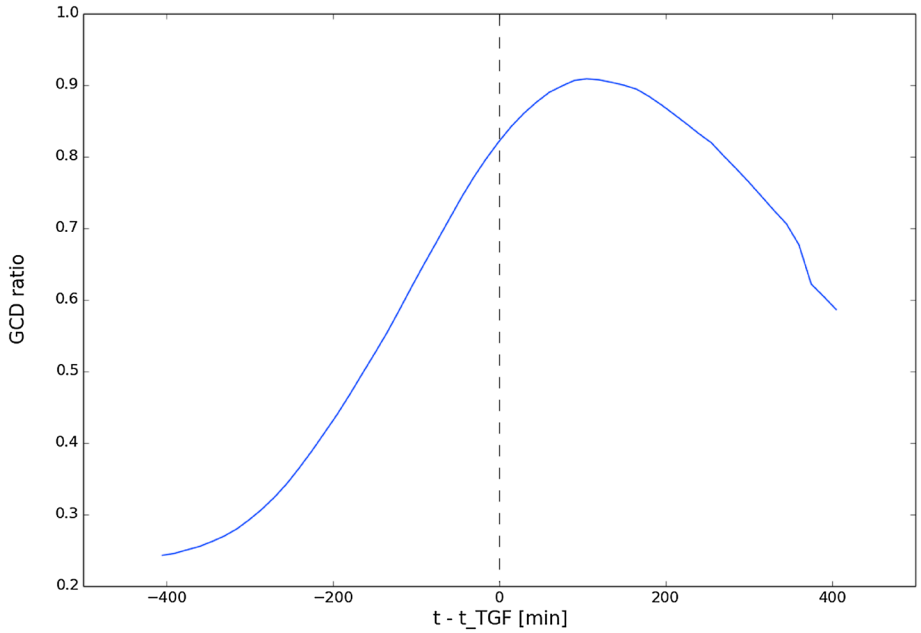

Figure 5. Cumulative plot of the GCD ratio, defined as the percentage of values satisfying a GCD $\leq 0°$ within a 6° sided square around the satellite footprint at the TGF time, for all the successive TGFs reported in this work. The general occurrence of our multiple TGFs seem to be associated to the increasing phase of the related thunderstorm.

multiple sferics have been found for our multiple TGF sample. Nevertheless, two sferics dated 13 April 2015 are particularly interesting, as they belong to the case of two pairs of consecutively detected TGFs, separated in time by three orbital passages: the first wave is associated to the first TGF of the first pair, while the second wave is associated to the second TGF of the second pair. This case is represented in Figure 4, together with the related meteorological image by MT-SAT2, which highlights the presence of a rising convective system, along the western coast of Sumatra.

Given the small number of associated sferics found for the multiple TGF sample, we performed a statistical analysis, in order to roughly determine in what thunderstorm phase our multiple TGFs tend to take place. We consider a 6° sided squared array, to take into consideration an uncertainty region whose size is comparable to the $\sim$ 700 km radius uncertainty circle around the footprint, and we study how the GCD ratio within this region changes with time. The GCD ratio is defined as the percentage of values within this array with GCD $\leq 0°$ and its variation in time reflects the storm evolution. Generally, regions with GCD $< 0°$ represent the presence of convection in the atmosphere. An increasing number of pixels with GCD $< 0°$ in time is then related to a convective system increasing its dimensions and height. The largest fraction of TGFs presented in this paper seem to occur during this phase, rather than in the decreasing successive phase, as shown in the cumulative plot of the GCD variation in time for all the multiple TGFs reported in Figure 5. This could have a physical explanation, meaning that TGFs are more likely to occur during this thunderstorm phase, but it could also be interpreted as the direct statistical consequence that a system with large dimensions has a higher lightning activity and a major spatial extension, making more probable for AGILE to observe multiple TGFs. In comparison, *Smith et al.* [2010] shows that a large fraction of RHESSI TGFs seem to take place just after the peak of lightning activity during thunderstorms.

5. Discussion and Conclusions

Systematic enhancements in the distribution of waiting times are expected, as TGFs do not occur randomly in space and time all over the globe. Extended thunderstorm systems in the tropics are active for several hours, clustering mostly over continents: A satellite overpassing a certain geographic region, where a large convective zone is present, will reasonably detect more events coming from the same zone, either during the same passage or during the successive overpasses. In the first RHESSI catalog, *Grefenstette et al.* [2009] shows an orbital resonance in the waiting time distribution of 591 TGFs, viewed as a confirmation that single thunderstorms are capable of producing multiple TGFs. However, given the higher-inclination orbit, RHESSI

Table 1. List of All 79 Detections of Repeated TGFs Coming From the Same Spatially Limited Geographic Region and Detected by the AGILE Satellite With the Standard Onboard Configuration[a]

Date	UTC	Δt (min)	Δx (km)	OP	S
3/4/2009	07:53:44				
3/4/2009	11:17:45	204	56	2	
6/11/2009	19:55:46				
6/11/2009	21:37:25	102	185	1	
6/11/2009	23:18:47	101	283	2	
22/11/2009	12:01:02				
22/11/2009	13:43:08	102	63	1	
13/4/2010	07:33:19				
13/4/2010	12:39:49	306	225	3	
5/11/2010	20:25:13				
5/11/2010	22:06:56	102	142	1	
5/11/2010	23:48:53	102	73	2	
18/3/2012	18:01:42				
18/3/2012	19:44:02	102	253	1	
10/10/2012	15:29:41				
10/10/2012	17:11:30	102	118	1	
20/11/2012	11:03:55				
20/11/2012	11:03:59	0	26	0	
8/12/2012	22:59:55				
9/12/2012	02:23:46	204	231	2	
18/12/2012	16:48:10				
18/12/2012	18:29:09	101	280	1	
26/2/2013	03:48:03				
26/2/2013	03:48:30	0	177	0	
14/3/2013	20:45:45				
15/3/2013	00:08:39	203	235	2	
23/3/2013	01:33:45				
23/3/2013	03:15:34	102	102	1	
25/3/2013	16:21:53				
25/3/2013	19:44:43	203	264	2	
19/4/2013	15:51:13				
19/4/2013	15:51:48	1	228	0	
1/12/2013	14:20:03				
1/12/2013	14:20:26	0	149	0	
2/12/2013	12:21:22				
2/12/2013	12:21:34	0	82	0	
31/10/2014	19:06:07				
31/10/2014	22:28:17	202	104	2	
31/10/2014	22:28:50	1	218	3	
24/3/2015	05:15:28				
24/3/2015	08:37:51	202	276	2	
24/3/2015	10:18:52	101	123	1	
24/3/2015	13:41:15				
24/3/2015	13:41:42	0	178	0	
1/4/2015	15:19:59				
1/4/2015	22:03:54	404	228	4	
4/4/2015	11:12:30				+94 μs

Table 1. (continued)

Date	UTC	Δt (min)	Δx (km)	OP	S
4/4/2015	11:12:52	0	141	0	
7/4/2015	08:13:16				+3 μs
7/4/2015	09:53:50	101	164	1	
8/4/2015	13:56:21				
8/4/2015	13:56:29	0	50	0	
13/4/2015	12:06:36				−30 μs
13/4/2015	12:06:53	0	111	0	
13/4/2015	17:09:11				
13/4/2015	17:09:54	1	290	0	+120 μs
15/4/2015	04:04:08				
15/4/2015	04:04:48	1	259	0	
15/4/2015	19:38:49				
15/4/2015	21:19:15	100	218	1	
19/4/2015	15:46:41				
19/4/2015	15:47:02	0	137	0	
19/4/2015	15:49:04				
19/4/2015	15:49:46	1	281	1	
20/4/2015	10:20:44				
20/4/2015	12:02:00	101	132	1	
28/4/2015	11:52:35				
28/4/2015	11:52:41	0	42	0	
6/5/2015	11:38:43				
6/5/2015	11:38:55	0	83	0	
6/5/2015	11:39:52				
6/5/2015	15:02:01	202	116	2	
8/5/2015	19:35:34				
8/5/2015	22:57:26	202	213	2	
14/5/2015	14:45:46				
14/5/2015	18:07:12	201	271	2	
21/5/2015	18:23:59				
21/5/2015	21:46:12	202	266	2	
25/5/2015	13:12:12				
25/5/2015	14:53:31	101	163	1	
26/5/2015	19:52:37				+41 μs
27/5/2015	00:55:09	303	267	3	
28/5/2015	10:31:55				
28/5/2015	10:32:07	0	78	0	
28/5/2015	13:31:11				
28/5/2015	13:31:37	0	175	0	
28/5/2015	15:12:12	101	151	1	
29/5/2015	13:30:45				
29/5/2015	15:12:15	102	238	1	
30/5/2015	15:58:54				
30/5/2015	15:59:21	0	175	0	
1/6/2015	07:06:35				
1/6/2015	08:46:57	100	243	1	
8/6/2015	15:15:12				
8/6/2015	16:56:36	101	211	1	

Table 1. (continued)

Date	UTC	Δt (min)	Δx (km)	OP	S
8/6/2015	16:56:36				
8/6/2015	23:40:19	404	279	4	
8/6/2015	23:42:20				
9/6/2015	03:04:26	202	216	2	
18/6/2015	12:26:37				
18/6/2015	15:48:25	202	156	2	
18/6/2015	15:48:25				
18/6/2015	15:48:58	1	221	1	
20/6/2015	14:52:43				
20/6/2015	14:52:55	0	82	0	−20 μs
20/6/2015	16:34:14	101	203	1	
31/7/2015	16:34:21				
31/7/2015	18:15:04	101	77	1	
15/8/2015	19:26:49				
15/8/2015	21:07:23	101	167	1	
24/8/2015	23:40:29				
24/8/2015	23:40:47	0	117	0	
25/8/2015	01:21:55	101	157	1	
30/8/2015	00:19:38				
30/8/2015	01:59:57	100	230	1	
29/9/2015	18:41:01				
29/9/2015	18:41:18	0	113	0	
29/9/2015	18:41:35	0	113	0	
5/10/2015	14:12:53				
5/10/2015	14:13:24	1	204	0	
8/10/2015	12:47:56				
8/10/2015	16:09:45	202	217	2	
12/10/2015	12:38:01				
12/10/2015	19:21:05	403	128	4	
14/10/2015	16:44:25				
14/10/2015	20:06:20	202	230	2	
17/10/2015	06:53:55				
17/10/2015	10:15:19	201	255	2	
22/10/2015	18:01:01				
22/10/2015	23:03:04	302	219	3	
25/10/2015	11:53:38				
25/10/2015	15:15:13	202	124	2	
5/11/2015	14:43:53				
5/11/2015	14:43:58	0	32	0	
13/11/2015	14:18:11				
13/11/2015	15:58:22	100	269	1	
14/11/2015	09:10:32				
14/11/2015	14:12:57	302	282	3	
22/11/2015	16:42:18				
22/11/2015	16:42:18	0	0	0	
8/12/2015	09:26:40				
8/12/2015	09:26:40	0	0	0	
10/12/2015	10:11:13				

Table 1. (continued)

Date	UTC	Δt (min)	Δx (km)	OP	S
10/12/2015	13:32:13	201	242	2	
14/12/2015	13:20:45				
14/12/2015	13:20:45	0	0	0	
5/1/2016	22:27:54				
6/1/2016	00:08:37	101	87	1	
8/1/2016	22:39:05				
9/1/2016	00:20:35	101	286	1	
12/1/2016	05:37:34				
12/1/2016	05:38:02	0	187	0	
15/1/2016	00:44:36				
15/1/2016	00:44:36	0	0	0	
18/1/2016	09:49:54				
18/1/2016	11:30:38	101	75	1	
23/2/2016	13:12:18				
23/2/2016	13:12:18	0	0	0	
7/3/2016	05:59:15				
7/3/2016	07:40:39	101	275	1	
9/3/2016	22:34:55				
10/3/2016	01:56:41	202	265	0	
10/3/2016	12:29:35				
10/3/2016	14:10:01	100	125	1	
10/3/2016	15:50:07	100	258	2	
11/3/2016	15:19:27				
11/3/2016	15:19:27	0	0	0	

[a] Among them, 28 systems produced multiple TGFs detected during the same orbital passage, while the remaining 51 systems produced multiple TGFs observed throughout successive passages. Columns show date and time of the TGFs, together with time separation, spatial distance, orbital passage, and presence of associated WWLLN sferics. Several cases of TGFs detected either during the same passage and throughout the successive overpasses are present.

does not observe orbital resonances for the successive $n > 1$ overpasses. We search throughout this data set of repeated events evidences of multiple TGFs-producing thunderstorms.

The quasi-equatorial orbit and the high detection capability of AGILE represent unique features for what concerns the monitoring of a specific geographic region: this puts AGILE in a privileged position, with respect to other current TGF detecting satellites, such as RHESSI and Fermi, whose orbital inclination is slightly higher, making the satellite able to observe more TGFs coming from the same convective region, even during successive overpasses. The study of the waiting times distribution between successively detected events highlights evident enhancements, either within 1 min or at the successive orbital resonances. We present the observation of 79 cases of convective systems producing more TGFs, listed in Table 1: in particular, 28 out of these systems produced more TGFs, detected by AGILE during the same passage, and 51 out of these systems lasted several hours, producing events that have been detected up to 4 overpasses after. Moreover, three mixed cases of repeated TGFs from the same thunderstorm system detected either during the same passage and at successive passages have been observed. Meteorological images acquired by geostationary satellites (Meteosat-10, Himawari-7, and GOES 13/15) included in the AGILE meteoretrieving pipeline show the presence of convective systems in the region of interest, frequently lasting several hours in order to produce more TGFs detected at successive passages. These data show that the underlying thunderstorms producing multiple TGFs exhibit very different extensions and structures, quite consistent with the results found by *Splitt et al.* [2010] and *Chronis et al.* [2016], suggesting that there are no privileged types of thunderstorm for TGF production.

A statistical study on the variation in time of the GCD algorithm was carried out: multiple TGFs are detected even after several hours, during successive passages, and cannot therefore be univocally associated to a specific phase of the thunderstorm evolution, the cumulative distribution of the multiple TGFs occurrence times shows that these events tend to take place in the final part of the thunderstorm development, when the system is increasing its height and size. This result is contrary to what is obtained by *Smith et al.* [2010], who found the peak of TGF production during a thunderstorm is when the lightning flash rate is decreasing. However, it is worth noticing that this result could merely be interpreted as a direct statistical consequence of the fact that thunderstorms in their largest size and highest vertical extension phase make more probable for a satellite to observe multiple TGFs during its overpass, with no substantial physical meaning.

As explained in section 2, sferic counterparts to AGILE TGFs were found only for 3 months activity, between 23 March 2015 and 23 June 2015: as a consequence, the search for sferics in the WWLLN database for our multiple TGF sample produced just six cross correlations, which unfortunately match individual TGFs of the multiple TGF subsets. Nevertheless, for case 13 April 2015, two sferics have been found, related to two TGF pairs, coming from the same convective system and separated in time by three orbital passages, representing the first evidence that a single thunderstorm is capable of producing more TGFs throughout its lifetime. The results of this study could be interpreted as the consequence that, in principle, every thunderstorm produces a large number of TGFs throughout its lifetime, along with the intrinsic lightning production: thunderstorm type, size, and altitude could play a role in making the TGF detection easier or harder for a satellite, but not in a significant way. This work not only represents a further confirmation of the efficiency of the AGILE satellite as a TGF detector, both for its quasi-equatorial orbit and the high sensitivity to these events, but it is also the first proof that single thunderstorm systems can produce multiple TGFs throughout their entire lifetime.

Acknowledgments
GILE is a mission of the Italian Space Agency (ASI), with coparticipation of INAF (Istituto Nazionale di Astrofisica) and INFN (Istituto Nazionale di Fisica Nucleare). This work was carried out in the frame of the ASI-INAF agreement I/028/12/0. The multiple TGF sample presented in this work is a part of the AGILE TGF database, publicly available online at the ASI Science Data Center (ASDC) website (http://www.asdc.asi.it/mcaletgfcat/). The meteorological data used for this work have been provided by the European Organisation for the Exploitation of Meteorological Satellites (EUMETSAT), and the lightning location data have been provided by the World Wide Lightning Location Network (WWLLN). All other AGILE MCAL and meteorological data used for this work are available, upon request, from A. Ursi (alessandro.ursi@iaps.inaf.it).

References

Briggs, M. S., et al. (2010), First results on terrestrial gamma ray flashes from the Fermi Gamma-ray Burst Monitor, *J. Geophys. Res.*, *115*, A07323, doi:10.1029/2009JA015242.

Briggs, M. S., et al. (2013), Terrestrial gamma-ray flashes in the Fermi era: Improved observations and analysis methods, *J. Geophys. Res.*, *118*, 3805–3830, doi:10.1002/jgra.50205.

Chronis, T., et al. (2016), Characteristics of thunderstorms that produce terrestrial gamma ray flashes, *Bull. Am. Meteorol. Soc.*, *97*, 639–653, doi:10.1175/BAMS-D-14-00239.1.

Connaughton, V., et al. (2010), Associations between Fermi Gamma-ray Burst Monitor terrestrial gamma ray flashes and sferics from the World Wide Lightning Location Network, *J. Geophys. Res.*, *115*, A12307, doi:10.1029/2010JA015681.

Connaughton, V., et al. (2013), Radio signals from electron beams in terrestrial gamma ray flashes, *J. Geophys. Res.*, *118*, 2313–2320, doi:10.1029/2012JA018288.

Cummer, S. A., et al. (2014), The source altitude, electric current, and intrinsic brightness of terrestrial gamma ray flashes, *Geophys. Res. Lett.*, *41*, 8586–8593, doi:10.1002/2014GL062196.

Dwyer, J. R. (2008), Source mechanisms of terrestrial gamma-ray flashes, *J. Geophys. Res.*, *113*, D10103, doi:10.1029/2007JD009248.

Dwyer, J. R. (2012), The relativistic feedback discharge model of terrestrial gamma ray flashes, *J. Geophys. Res.*, *117*, A02308, doi:10.1029/2011JA017160.

Dwyer, J. R., and D. M. Smith (2005), A comparison between Monte Carlo simulations of runaway breakdown and terrestrial gamma-ray flash observations, *Geophys. Res. Lett.*, *32*, L22804, doi:10.1029/2005GL023848.

Fabró, F., et al. (2015), Analysis of global Terrestrial Gamma Ray Flashes distribution and special focus on AGILE detections over South America, *J. Atmos. Sol. Terr. Phys.*, *124*, 10–20, doi:10.1002/jgra.50188.

Fishman, G. J., et al. (1994), Discovery of intense gamma-ray flashes of atmospheric origin, *Science*, *264*, 1313–1316.

Fuschino, F., et al. (2011), High spatial resolution correlation of AGILE TGFs and global lightning activity above the equatorial belt, *Geophys. Res. Lett.*, *38*(14), L14806, doi:10.1029/2011GL047817.

Grefenstette, B. W., D. M. Smith, B. J. Hazelton, and L. I. Lopez (2009), First RHESSI terrestrial gamma ray flash catalog, *J. Geophys. Res.*, *114*, A02314, doi:10.1029/2008JA013721.

Gurevich, A. V., G. M. Milikh, and R. Roussel-Dupre (1992), Runaway electron mechanism of air breakdown and preconditioning during a thunderstorm, *Phys. Lett. A*, *165*, 463–468, doi:10.1016/0375-9601(92)90348-P.

Labanti, C., et al. (2009), Design and construction of the Mini-Calorimeter of the AGILE satellite, *Nucl. Instrum. Methods Phys. Res. A*, *598*, 470–479, doi:10.1016/j.nima.2008.09.021.

Lu, G., et al. (2010), Lightning mapping observation of a terrestrial gamma-ray flash, *Geophys. Res. Lett.*, *37*, L11806, doi:10.1029/2010GL043494.

Marisaldi, M. (2010a), Detection of terrestrial gamma ray flashes up to 40 MeV by the AGILE satellite, *J. Geophys. Res.*, *115*, A00E13, doi:10.1029/2009JA014502.

Marisaldi, M., et al. (2010b), Gamma-ray localization of terrestrial gamma-ray flashes, *Phys. Rev. Lett.*, *105*(12), 128501, doi:10.1103/PhysRevLett.105.128501.

Marisaldi, M., et al. (2014), *The First AGILE Low-Energy (<30 MeV) Terrestrial Gamma-Ray Flashes Catalog*, 11326 pp., EGU General Assembly 2014, held 27 April – 2 May, 2014, Vienna.

Marisaldi, M., et al. (2015), Enhanced detection of terrestrial gamma-ray flashes by AGILE, *Geophys. Res. Lett.*, *42*, 9481–9487, doi:10.1002/2015GL066100.

Martin, D. W., R. A. Kohrs, F. R. Mosher, C. M. Medaglia, and C. Adamo (2008), Over-ocean validation of the global convective diagnostic, *J. Appl. Meteorol. Climatol.*, *47*, 525–543, doi:10.1175/2007JAMC1525.1.

Mosher, M. (2001), A satellite diagnostic of global convection, *Astron. Astrophys.*, *502*, 995–1013, doi:10.1051/0004-6361/200810527.

Shao, X. M., et al. (2010), A closer examination of terrestrial gamma-ray flash-related lightning processes, *J. Geophys. Res.*, *115*, A00E30, doi:10.1029/2009JA014835.

Splitt, M. E., et al. (2010), Thunderstorm characteristics associated with RHESSI identified terrestrial gamma ray flashes, *J. Geophys. Res. Atmos.*, *115*, A00E38, doi:10.1029/2009JA014622.

Smith, D. M., et al. (2005), Terrestrial gamma-ray flashes observed up to 20 MeV, *Science*, *307*, 1085–1088.

Smith, J. R., et al. (2010), Terrestrial gamma ray flashes correlated to storm phase and tropopause height, *J. Geophys. Res.*, *115*(A14), A00E49, doi:10.1029/2009JA014853.

Stanley, M. A., et al. (2006), A link between terrestrial gamma-ray flashes and intracloud lightning discharges, *Geophys. Res. Lett.*, *33*, L06803, doi:10.1029/2005GL025537.

Tavani, M., and othes (2009), The AGILE mission, *Astron. Astrophys.*, *502*, 995–1013, doi:10.1051/0004-6361/200810527.

Tavani, M., et al. (2011), *Terrestrial Gamma-Ray Flashes at the highest energies as detected by AGILE*, Abstract AE24A-06 presented at 2011 Fall Meeting, AGU, San Francisco, Calif.